Research Square

Preprints are preliminary reports that have not undergone peer review.
They should not be considered conclusive, used to inform clinical practice,
or referenced by the media as validated information.

An Extended Multi-Source WEPI Framework for Mapping Wind Erosion Potential, Hotspots, and Priority Zones in Lorestan Province, Iran

Mostafa Ghasemzadeh Ortakand
University of Tehran
Meysam Bali
meysam.bali@aut.ac.ir
Amirkabir University of Technology

Research Article

Keywords: Wind erosion potential, remote sensing, Getis-Ord Gi*, Mann-Kendall trend, land degradation

Posted Date: November 4th, 2026

DOI: https://doi.org/10.21203/rs.3.rs-11255995/v1

License: This work is licensed under a Creative Commons Attribution 4.0 International License.
Read Full License

Additional Declarations: No competing interests reported.

An Extended Multi-Source WEPI Framework for Mapping Wind Erosion Potential, Hotspots, and Priority Zones in Lorestan Province, Iran

Mostafa Ghasemzadeh Ortakand[1], Meysam Bali[2]*.

Abstract

Wind erosion is a major driver of land degradation in dryland and seasonally exposed landscapes, yet its spatiotemporal dynamics remain insufficiently quantified in many mountainous semi-arid regions. This study developed an extended multi-source Wind Erosion Potential Index (WEPI) to assess wind erosion susceptibility in Lorestan Province, western Iran, during 2016–2025. The proposed framework integrated 120 monthly observations at 1000 m spatial resolution by combining vegetation protection loss, bare soil exposure, soil moisture dryness, land surface temperature, wind force, precipitation dryness, soil erodibility, topographic susceptibility, and land-cover exposure. The results revealed persistent moderate-to-high wind erosion potential, with annual mean WEPI ranging from 0.584 in 2020 to 0.605 in 2021 and a long-term mean of approximately 0.592. Approximately 95.31% of valid pixels were classified as moderate or higher risk, while summer exhibited the highest seasonal erosion potential, with a mean WEPI of 0.633. Component contribution analysis showed that bare soil exposure and vegetation protection loss together accounted for nearly 45.8% of the total WEPI. Spatial analyses identified 12,804 statistically significant hotspot pixels and 17,366 persistent high-risk pixels, indicating that chronic erosion susceptibility was more extensive than areas exhibiting significant temporal increases. The proposed framework provides a robust, reproducible, and transferable approach for identifying priority areas for wind erosion monitoring, land degradation assessment, and sustainable land management in semi-arid environments.

Keywords:

Wind erosion potential; remote sensing;Getis-Ord Gi*; Mann-Kendall trend;land degradation.

[1] School of Civil Engineering, University of Tehran, Tehran, Iran.
[2]* Assistant Professor, Department of Maritime Engineering, Amirkabir University of Technology, Tehran, Iran.
meysam.bali@aut.ac.ir

1. Introduction

Wind erosion is one of the major processes of land degradation in arid, semi-arid, and seasonally exposed landscapes. It removes fertile topsoil, depletes soil organic matter, reduces agricultural and rangeland productivity, and contributes to atmospheric dust loading. Wind erosion results from the interaction between erosive wind forces and land-surface resistance, which is governed by factors such as vegetation cover, soil moisture, soil texture, surface roughness, and bare soil exposure (Okin, 2008; Ravi et al., 2011; Shao et al., 2011). Recent research has further emphasized that erosion processes in dryland and transitional environments are strongly influenced by interactions among climatic forcing and multiple surface-related erosion processes (Yang et al., 2023).

Iran is highly vulnerable to wind erosion and dust-related land degradation because much of the country lies within the arid and semi-arid belt of Southwest Asia. Dust activity in Iran and neighboring regions is driven by a combination of drought, sparse vegetation cover, exposed soil surfaces, land degradation, and strong seasonal winds(Mohammadi et al., 2025). However, susceptibility to wind erosion is not confined to hyper-arid deserts. Transitional regions characterized by mountainous terrain, croplands, rangelands, and seasonally varying vegetation cover may also experience localized wind erosion when soils become dry and exposed(Khoshnoud et al., 2026). Lorestan Province in western Iran represents one such landscape. Although it is not among the driest provinces in Iran, its heterogeneous topography, diverse agricultural and rangeland systems, seasonal vegetation dynamics, and variable soil moisture conditions create spatially complex patterns of wind erosion potential.

Field-based assessments provide valuable local-scale information on wind erosion but are difficult to implement consistently across large regions and extended time periods. Moreover, wind erosion exhibits pronounced spatial heterogeneity and temporal variability, meaning that conventional field surveys may fail to capture seasonal changes, emerging hotspots, or long-term shifts in land-surface conditions. Remote sensing offers an effective alternative by enabling repeated and spatially continuous monitoring of the key environmental variables controlling wind erosion over broad areas. Furthermore, Google Earth Engine (GEE) facilitates large-scale geospatial analysis by providing access to cloud-based satellite imagery, climate reanalysis datasets, and distributed computing resources (Gorelick et al., 2017). Together, Sentinel-2, MODIS, SMAP, ERA5-Land,

CHIRPS, SoilGrids, SRTM, and ESA WorldCover provide complementary information for representing vegetation dynamics, soil moisture, land surface temperature, wind forcing, precipitation, soil properties, topography, and land-cover conditions (Drusch et al., 2012; Entekhabi et al., 2010; Farr et al., 2007; Funk et al., 2015; Hengl et al., 2017; Muñoz-Sabater et al., 2021; Zanaga et al., 2022).

Several previous studies have employed remote sensing and geographic information systems (GIS) to map land degradation, identify dust source areas, and assess erosion susceptibility. Recent studies in semi-arid landscapes have also demonstrated the effectiveness of long-term NDVI time series combined with Theil–Sen and Mann–Kendall analyses for characterizing spatial and temporal environmental dynamics (Chao et al., 2025). However, many existing approaches rely on static datasets, a limited number of input variables, or relatively short observation periods. Although these methods can identify generally vulnerable areas, they provide limited insight into temporal variability, persistent high-risk zones, statistically significant trends, and spatial clustering. Moreover, relatively few studies have integrated satellite, climate, soil, topographic, and land-cover datasets into a unified framework capable of simultaneously evaluating the spatial and temporal dynamics of wind erosion while identifying persistent hotspots and management-priority areas. Therefore, a comprehensive multi-source framework is needed to integrate these environmental controls into a spatially continuous and temporally consistent indicator of wind erosion risk.

The Wind Erosion Potential Index (WEPI) provides a practical framework for integrating multiple erosion-related variables into a single, interpretable metric. A baseline WEPI can be derived from vegetation condition, bare soil exposure, soil moisture deficit, land surface temperature, and wind speed, which collectively represent the interaction between land-surface resistance and erosive wind forces (Feizizadeh et al., 2025). To provide a more comprehensive assessment, additional variables including precipitation deficit, soil texture and organic matter content, topographic susceptibility, and land-cover conditions can also be incorporated. These variables strengthen the physical basis of the index and reduce its reliance on optical surface indicators alone. Because index-based models are sensitive to variable weighting, sensitivity analysis is essential for evaluating whether the spatial patterns of wind erosion potential remain robust under alternative weighting schemes(Feng et al., 2025).

In addition to index development, robust spatial and temporal analyses are essential for characterizing the dynamics of wind erosion potential. Monthly WEPI layers can be aggregated into seasonal and annual composites to evaluate temporal variability. The Theil–Sen estimator and the Mann–Kendall test are widely used in environmental trend analysis because they are non-parametric and robust to outliers (Kendall, 1975; Mann, 1945; Sen, 1968). Because pixel-wise trend analysis involves a large number of simultaneous statistical tests, applying a false discovery rate (FDR) correction helps reduce the likelihood of false-positive results (Benjamini & Hochberg, 1995). Spatial clustering can be further assessed using the Getis–Ord Gi* statistic, which identifies statistically significant hotspots and coldspots of high and low values, respectively (Getis & Ord, 1992). Collectively, these methods provide a statistically robust basis for detecting meaningful temporal trends and spatial clustering in wind erosion potential.

This study developed an extended multi-source Wind Erosion Potential Index (WEPI) framework to assess wind erosion potential in Lorestan Province, western Iran, during the period 2016–2025. The specific objectives were to: (1) develop monthly and long-term WEPI maps using satellite, reanalysis, climate, soil, topographic, and land-cover datasets; (2) classify wind erosion potential into meaningful risk categories; (3) analyze temporal trends using the Theil–Sen estimator and the Mann–Kendall test with false discovery rate (FDR) correction; (4) identify statistically significant hotspots and coldspots using the Getis–Ord Gi* statistic; (5) evaluate the sensitivity of the WEPI to alternative weighting schemes; and (6) delineate management-priority zones for land degradation monitoring and wind erosion mitigation. The proposed methodology provides a reproducible and transferable approach for identifying areas characterized by persistent, spatially clustered, and potentially increasing wind erosion potential.

2. Materials and Methods

2.1. Study Area and Workflow

This study assessed wind erosion potential in Lorestan Province, western Iran, during the period 2016–2025. Figure 1 shows the location of Lorestan Province, the spatial extent of the study area, and elevation variations across the study area. Lorestan is characterized by mountainous terrain, rangelands, agricultural lands, and pronounced seasonal variability in vegetation cover and soil

moisture, making it well suited for evaluating spatially heterogeneous wind erosion susceptibility. The workflow integrated satellite, reanalysis, climate, soil, topographic, and land-cover datasets to develop an extended Wind Erosion Potential Index (WEPI). Google Earth Engine (GEE) was used for data acquisition, preprocessing, monthly compositing, normalization, and raster export, whereas Python was used for post-processing, statistical analysis, hotspot detection, sensitivity analysis, map production, and reporting (Gorelick et al., 2017).

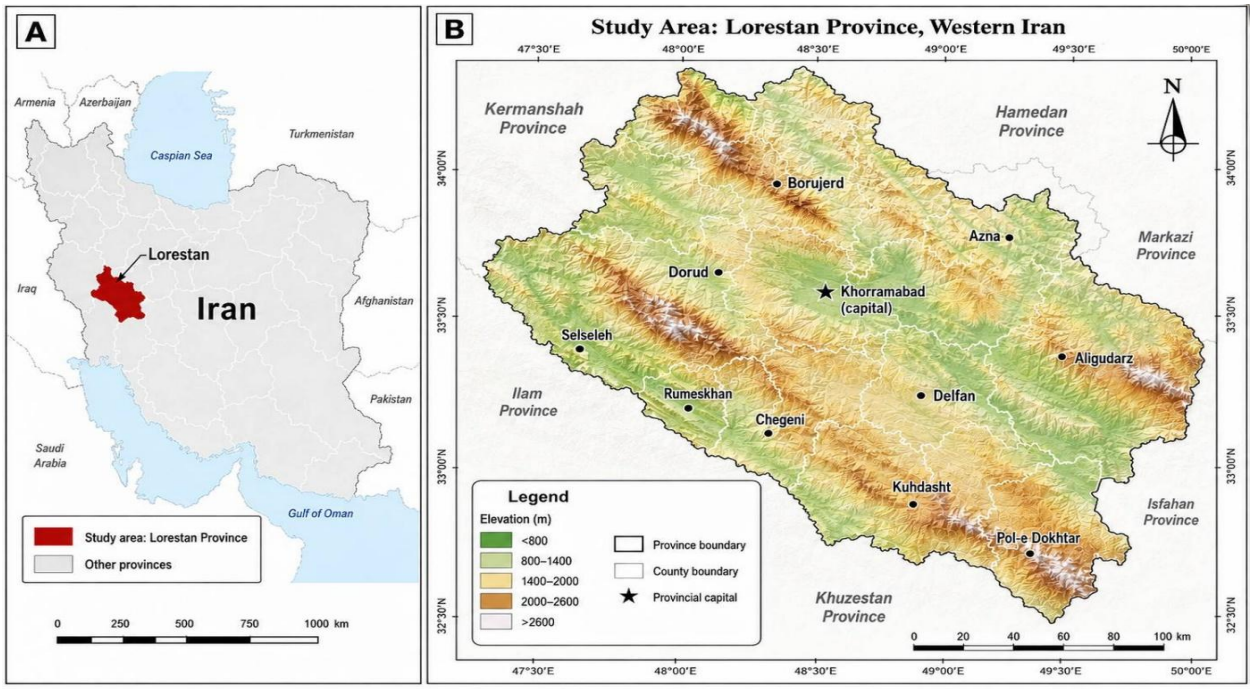


Figure 1 Location of Lorestan Province in western Iran, the spatial extent of the study area, and elevation variations across the study area.

2.2. Input Datasets and Preprocessing

Nine environmental factors were selected to represent the principal controls on wind erosion: vegetation condition, bare soil exposure, soil moisture deficit, land surface temperature (LST), wind force, precipitation deficit, soil erodibility, topographic susceptibility, and land-cover conditions. The original WEPI framework incorporated vegetation condition, bare soil exposure, soil moisture deficit, land surface temperature, and wind force, whereas precipitation deficit, soil erodibility, topographic susceptibility, and land-cover conditions were incorporated to improve the representation of climatic stress, soil vulnerability, terrain effects, and surface exposure.

Sentinel-2 provides high-resolution optical imagery for monitoring vegetation condition and bare soil exposure (Drusch et al., 2012). MODIS MOD11A2 was used to derive land surface temperature (LST) (Wan, 2006), SMAP provided near-surface soil moisture**,** ERA5-Land provided 10-m wind components (Muñoz-Sabater et al., 2021), CHIRPS provided precipitation data (Funk et al., 2015), SoilGrids provided soil texture and soil organic carbon information (Hengl et al., 2017), SRTM provided elevation and slope data (Farr et al., 2007), and ESA WorldCover provided land-cover information (Zanaga et al., 2022).

All datasets were clipped to the boundary of Lorestan Province**,** aggregated to monthly temporal resolution where necessary, and resampled to a common 1000-m spatial resolution. Sentinel-2 imagery was masked for clouds and cloud shadows before generating monthly median composites. ERA5-Land wind speed was calculated from the eastward (u) and northward (v) wind components as follows:

$$W = \sqrt{u^2 + v^2} \tag{1}$$

This preprocessing workflow followed the original methodology, including monthly compositing, resampling to a common spatial grid, gap filling, and valid-data mask generation. Table 1 summarizes the multi-source datasets used to construct the extended Wind Erosion Potential Index. The selected datasets represent the principal environmental controls on wind erosion, including vegetation condition, bare soil exposure, land surface temperature, soil moisture, wind, precipitation, soil properties, topography, and land-cover characteristics. These datasets differ in spatial and temporal resolution but were preprocessed and harmonized to produce a consistent monthly dataset at a common 1000 m spatial resolution for WEPI calculation.

Table 1. Input datasets used for WEPI construction.

Factor	Dataset	Resolution	Temporal scale	Derived variable
Vegetation	Sentinel-2 SR Harmonized	10–20 m	Monthly median	$NDVI/V_f$

Bare soil	Sentinel-2 SR Harmonized	10–20 m	Monthly median	BSI
LST	MODIS MOD11A2	1 km	8-day to monthly	LST_f
Soil moisture	SMAP SPL3SMP_E	9 km	Daily to monthly	SM_f
Wind	ERA5-Land	0.1° / ~9 km	Daily to monthly	W_f
Precipitation	CHIRPS	0.05° / ~5.6 km	Daily to monthly	P_{dry}
Soil	SoilGrids	250 m	Static	$SoilE$
Topography	SRTM DEM	~30 m	Static	$TopoF$
Land cover	ESA WorldCover	10 m	Static	LCF

2.3. WEPI Component Derivation and Normalization

Vegetation protection loss was derived from the Normalized Difference Vegetation Index (NDVI):

$$NDVI = \frac{NIR - Red}{NIR + Red} \quad (2)$$

Because sparse vegetation increases wind erosion susceptibility, NDVI was normalized and inverted to represent vegetation protection loss. Vegetation structure also modifies aerodynamic roughness and near-surface wind conditions, thereby affecting the resistance of grassland surfaces to wind erosion (Li et al., 2023).

$$V_f = 1 - NDVI_{norm} \quad (3)$$

Bare soil exposure was estimated using the Bare Soil Index (BSI):

$$BSI = \frac{(SWIR + Red) - (NIR + Blue)}{(SWIR + Red) + (NIR + Blue)} \quad (4)$$

Consistent with the original WEPI framework, NDVI and BSI were used to represent vegetation protection and bare soil exposure, respectively.

Soil moisture was converted into a soil moisture deficit factor:

$$SM_f = 1 - SM_{norm} \quad (5)$$

Land surface temperature and wind speed were normalized directly:

$$LST_f = LST_{norm} \quad (6)$$

$$W_f = W_{norm} \quad (7)$$

Precipitation was converted into a precipitation deficit factor:

$$P_{dry} = 1 - P_{norm} \quad (8)$$

Soil erodibility was estimated from normalized sand, silt, clay, and soil organic carbon (SOC) contents:

$$SoilE = 0.35Sand_{norm} + 0.35Silt_{norm} + 0.20(1 - Clay_{norm}) + 0.10(1 - SOC_{norm}) \quad (9)$$

Topographic susceptibility was derived from normalized slope values obtained from the SRTM digital elevation model (DEM):

$$TopoF = 1 - Slope_{norm} \quad (10)$$

Land-cover exposure was assigned using ESA WorldCover land-cover classes, with bare or sparsely vegetated areas receiving the highest exposure scores, whereas forests, water bodies, wetlands, and permanent snow or ice received lower scores.

All variables were normalized to a common 0–1 scale using percentile normalization:

$$X_{norm} = \frac{X - P_2}{P_{98} - P_2} \quad (11)$$

$$X_{norm} = clamp(X_{norm}, 0,1)$$

where P_2 and P_{98} represent the 2nd and 98th percentiles, respectively. Percentile normalization minimizes the influence of outliers while ensuring that all variables are represented on a comparable scale. Consistent with the original WEPI framework, all variables were normalized before index construction.

2.4. WEPI Construction, Classification, and Sensitivity Analysis

A baseline five-factor WEPI was calculated as:

$$WEPI_5 = 0.30V_f + 0.25BSI + 0.20SM_f + 0.15LST_f + 0.10W_f \quad (12)$$

This weighting scheme was adopted from the original WEPI framework, in which vegetation protection and bare soil exposure received the highest weights because they exert the greatest influence on surface protection and the availability of erodible material.

The extended WEPI was calculated as:

$$WEPI_{ext} = 0.22V_f + 0.20BSI + 0.14SM_f + 0.10LST_f + 0.10W_f + 0.08P_{dry} + 0.08SoilE + 0.04TopoF + 0.04LCF \quad (13)$$

This formulation integrates vegetation condition, bare soil exposure, soil moisture deficit, land surface temperature, wind force, precipitation deficit, soil erodibility, topographic susceptibility, and land-cover exposure into a single composite index. All weighting coefficients were normalized so that their sum equaled 1.0.

Following the equal-interval wind erosion susceptibility classification applied by Gholami et al. (2024), normalized WEPI values were divided into five classes ranging from very low to very high, as presented in Table 2.

Table 2. Classification of Wind Erosion Potential Index values into five erosion-risk classes based on the equal-interval thresholds used by Gholami et al. (2024).

WEPI range	Risk class
0.0–0.2	Very low
0.2–0.4	Low
0.4–0.6	Moderate
0.6–0.8	High
0.8–1.0	Very high

These risk classes were applied to monthly, seasonal, annual, and long-term mean WEPI maps to facilitate spatial interpretation and temporal comparison.

To evaluate the robustness of the proposed framework, sensitivity analysis was performed using five weighting schemes: the baseline five-factor scheme, the extended balanced scheme, the equal-weight extended scheme, the surface-driven scheme, and the climate-driven scheme. For each scheme, the mean WEPI, the proportion of areas classified as moderate-or-higher, high-or-higher, and very high risk, together with the spatial correlation relative to the primary WEPI map, were calculated. Areas that remained consistently classified as high risk across all weighting schemes were considered robust wind erosion hotspots.

2.5. Spatiotemporal Analysis, Hotspots, and Robustness Assessment

Monthly WEPI maps were aggregated into annual and seasonal products:

$$WEPI_{annual,y} = \frac{1}{n_y} \sum_{m=1}^{n_y} W\,EPI_{y,m} \tag{14}$$

where n_y is the number of valid monthly observations in year yyy. Seasonal composites were generated for winter (DJF), spring (MAM), summer (JJA), and autumn (SON). For each time step, regional summary statistics, including the mean, median, standard deviation, minimum, maximum, and selected percentiles, were calculated.Temporal trends were evaluated using the Theil–Sen slope estimator and the Mann–Kendall test, which are widely applied in non-parametric environmental trend analysis because of their robustness to outliers (Mann, 1945; Sen, 1968; Kendall, 1975).

A common pitfall in pixel-wise environmental trend analysis is the inflation of Type I errors (false positives) due to multiple simultaneous hypothesis testing. By incorporating the Benjamini-Hochberg false discovery rate (FDR) correction alongside the Mann-Kendall test, this framework rigorously controls for spurious temporal trends that often plague large-scale remote sensing studies. Furthermore, the integration of the Getis-Ord Gi* statistic elevates the spatial analysis beyond simple pixel counting. Instead of merely identifying isolated pixels with high erosion potential, this approach statistically delineates contiguous hotspot clusters. This ensures that the identified priority zones represent genuinely cohesive areas of vulnerability rather than random spatial noise, providing a much stronger basis for subsequent land management interventions.

Consistent with the original WEPI methodology, these methods were applied on a pixel-by-pixel basis. The Theil–Sen slope was calculated as:

$$\beta = median\left(\frac{WEPI_j - WEPI_i}{t_j - t_i}\right), \quad j > i \tag{15}$$

Positive values indicate increasing erosion potential, while negative values indicate decreasing potential. The Mann-Kendall statistic was calculated as:

$$S = \sum_{i=1}^{n-1} \sum_{j=i+1}^{n} sign\left(WEPI_j - WEPI_i\right) \tag{16}$$

Pixels with ($p < 0.05$) were considered statistically significant. Because many pixels were tested simultaneously, Benjamini-Hochberg false discovery rate correction was applied (Benjamini & Hochberg, 1995).

Endpoint change was calculated as:

$$\Delta WEPI = WEPI_{2025} - WEPI_{2016} \tag{17}$$

Positive values indicate increasing wind erosion potential, whereas negative values indicate decreasing potential. Unlike the Mann–Kendall trend analysis, endpoint differencing reflects only the net change between the first and last years and is therefore sensitive to the selected time interval(Saeedi Nazarlu et al., 2026)..

High-risk persistence was calculated as:

$$Persistence = \frac{N(WEPI \geq 0.6)}{N_{total}} \tag{18}$$

where $N(WEPI \geq 0.6)$ is the number of valid observations classified as high or very high risk.

Spatial clustering was evaluated using the Getis-Ord Gi* statistic (Getis & Ord, 1992), which identifies statistically significant hotspots and coldspots. The original study also used Getis-Ord Gi* for hotspot analysis. Pixels with $Gi^*Z > 1.96$ were classified as hotspots, while pixels with $Gi^*Z < -1.96$ were classified as coldspots.

Finally, a management-priority index was calculated by integrating high mean WEPI, hotspot occurrence, significant increasing trends, positive endpoint change, high-risk persistence, and data quality:

$$Priority = 2(HR) + 2(HS) + 2(SIT) + 1(PD) + 2(HP) - 1(LQ) \quad (19)$$

The complete methodological workflow is summarized in Figure 2.

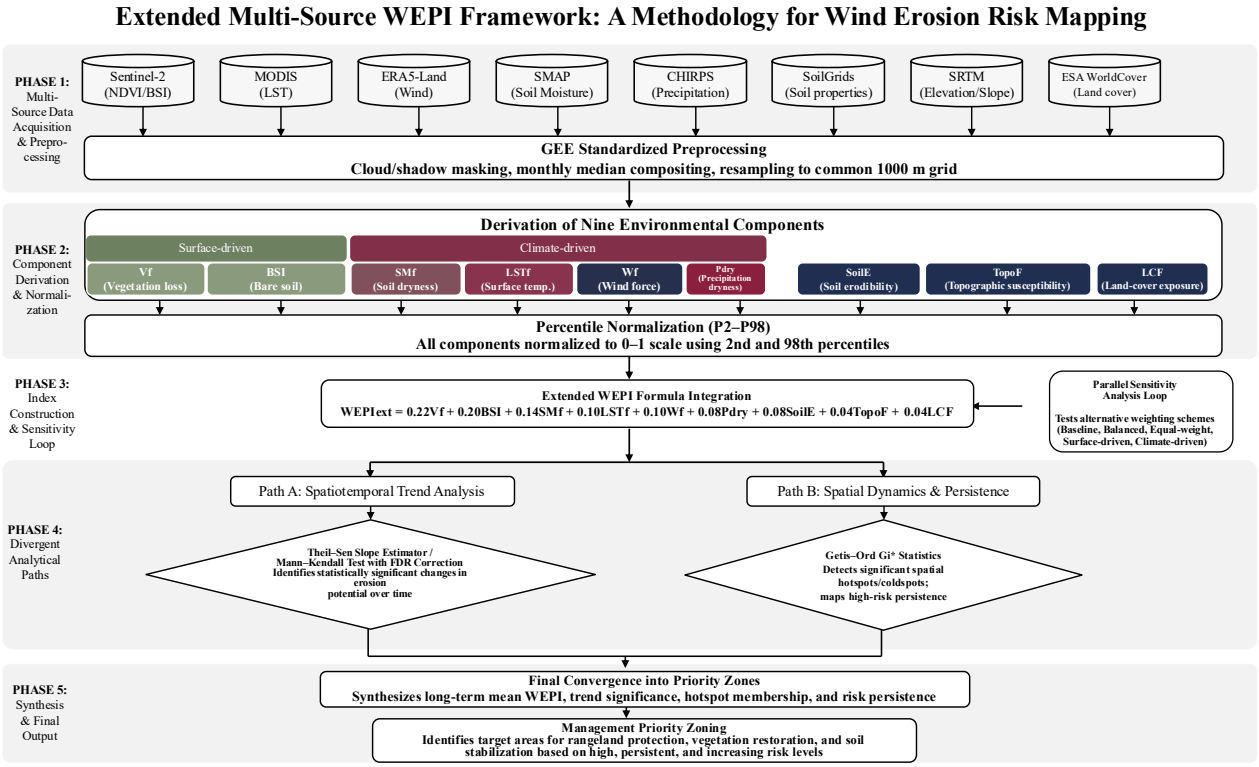


Figure 2. Methodological workflow for constructing the multi-source WEPI, performing spatiotemporal analyses, hotspot detection, sensitivity analysis, and delineating management-priority zones.

3. Results

3.1. Output completeness and general WEPI pattern

The final WEPI workflow was implemented for Lorestan Province during 2016–2025 using the extended balanced WEPI model at a 1000-m spatial resolution. The analysis generated 120 monthly WEPI maps, annual composites, long-term mean and standard deviation maps, endpoint change maps, Theil–Sen slope estimates, Mann–Kendall significance maps, false discovery rate

(FDR)-corrected trend maps, Getis–Ord Gi* hotspot maps, high-risk persistence maps, and management-priority maps. The processing completeness and primary WEPI outputs are summarized in Table 3.

As shown in Figure 3, wind erosion potential was widely distributed across Lorestan Province. The long-term mean WEPI was 0.592**,** with pixel values ranging from 0.298 to 0.834**,** indicating that most of the province exhibited moderate to high wind erosion potential**.** Elevated WEPI values formed extensive and spatially connected zones rather than isolated patches, highlighting the broad spatial distribution of wind erosion susceptibility across the province.

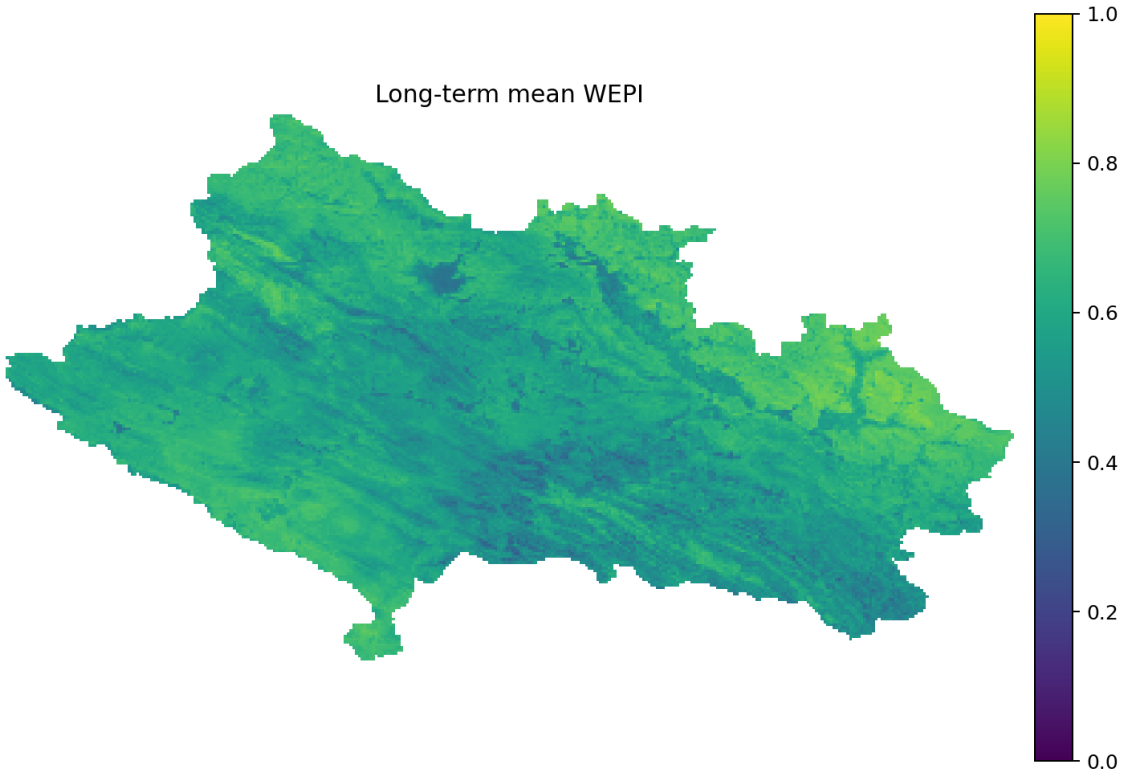


Figure 3. Long-term mean Wind Erosion Potential Index (WEPI) across Lorestan Province during 2016–2025.

Table 3. Summary of WEPI processing and primary outputs

Indicator	Result
Study area	Lorestan Province, Iran
Study period	2016–2025
Monthly periods processed	120
Spatial resolution	1000 m
Primary WEPI model	Extended balanced
Progress records	252
Failed exports	0
Valid pixels in main annual rasters	34,689
Long-term mean WEPI	0.592
Long-term WEPI standard deviation	0.080

3.2. Annual and monthly variation of WEPI

Annual mean WEPI values were relatively stable during the study period, ranging from 0.584 in 2020 to 0.605 in 2021. The annual mean increased from 0.589 in 2016 to 0.601 in 2025, but the magnitude of change was small. This indicates persistent moderate-to-high wind erosion potential rather than strong interannual instability. The annual statistics are summarized in Table 4, and the temporal pattern is shown in Figure 4.

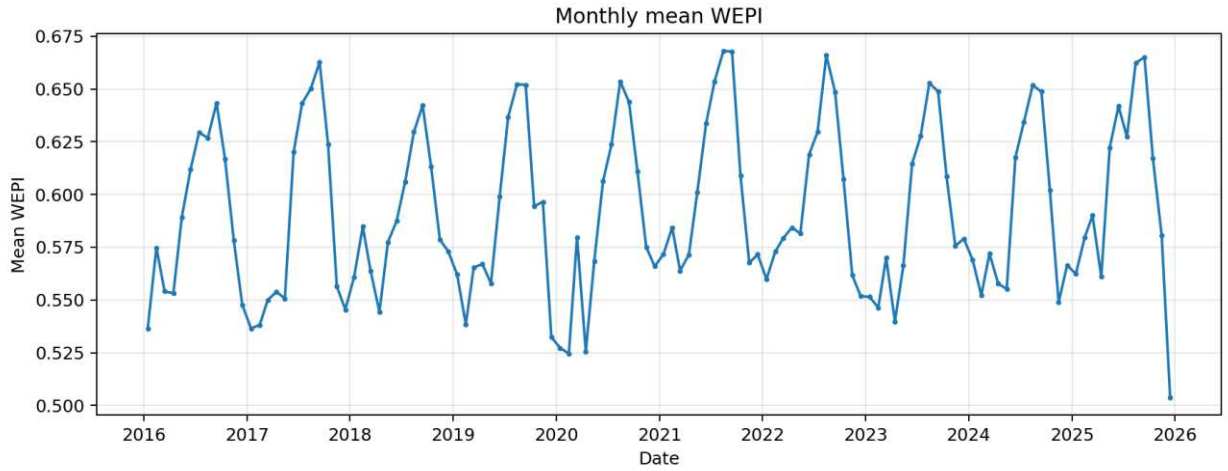


Figure 4. Temporal variation of mean WEPI in Lorestan Province during 2016–2025.

Table 4. Annual WEPI statistics for Lorestan Province, 2016–2025.

Year	Mean	Median	Std. dev.	Min	Max	P5	P95
2016	0.589	0.592	0.084	0.267	0.831	0.444	0.725
2017	0.586	0.588	0.083	0.286	0.859	0.444	0.718
2018	0.588	0.585	0.077	0.326	0.835	0.467	0.721
2019	0.588	0.589	0.080	0.294	0.809	0.452	0.714
2020	0.584	0.589	0.082	0.273	0.823	0.440	0.707
2021	0.605	0.606	0.084	0.307	0.860	0.463	0.739
2022	0.597	0.604	0.085	0.280	0.805	0.446	0.719
2023	0.590	0.589	0.084	0.290	0.853	0.452	0.734
2024	0.590	0.590	0.085	0.293	0.848	0.450	0.732
2025	0.601	0.608	0.083	0.278	0.849	0.452	0.726

At the monthly scale, WEPI showed a clear seasonal cycle. The lowest monthly mean occurred in December 2025 with WEPI = 0.504, while the highest monthly mean occurred in August 2021 with WEPI = 0.668. Monthly climatology increased from winter and spring toward summer, with the highest average values in August and September.

3.3. Risk-class distribution and seasonal variability

The WEPI risk classification confirmed that moderate-to-high erosion potential dominated the valid study area. Across the monthly outputs, the mean valid-area share was 48.49% moderate, 44.08% high, and 2.74% very high. Therefore, approximately 95.31% of the valid area was classified as moderate or higher wind erosion potential. Low and very-low classes represented only 4.67% and 0.02%, respectively.The corresponding risk-class percentages and seasonal mean WEPI values are summarized in Table 5. Figure 5 illustrates the distribution of WEPI risk classes across Lorestan Province during 2016–2025.

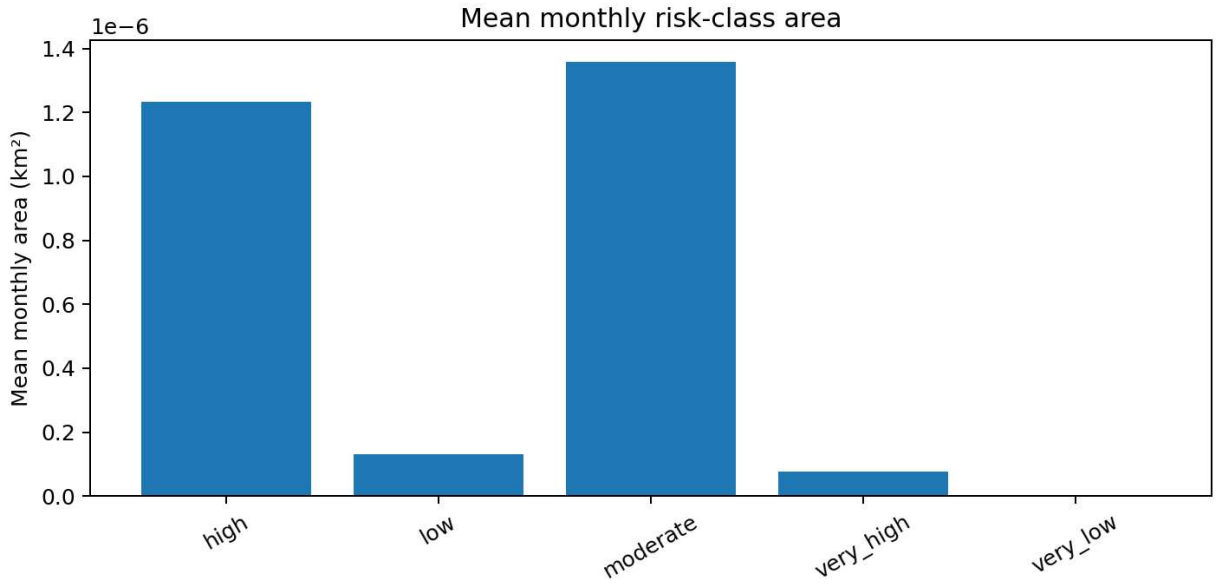


Figure 5. WEPI risk-class distribution

Table 5. Mean risk-class distribution and seasonal WEPI statistics.

Category	Result
Very low risk area	0.02%
Low risk area	4.67%
Moderate risk area	48.49%
High risk area	44.08%
Very high risk area	2.74%

Category	Result
Moderate-or-higher risk area	95.31%
Mean DJF WEPI	0.556
Mean MAM WEPI	0.567
Mean JJA WEPI	0.633
Mean SON WEPI	0.612

Seasonal analysis showed that erosion potential was highest during the warm and dry seasons. Mean WEPI reached 0.633 in JJA, followed by 0.612 in SON, while lower values were observed in DJF and MAM. This indicates that summer and early autumn are the most critical periods for wind erosion monitoring in Lorestan.

3.4. Component contribution and sensitivity analysis

Component contribution analysis indicated that the extended WEPI was primarily influenced by vegetation condition and surface exposure. As shown in Figure 6 and Table 6, bare soil exposure (BSI) made the largest weighted contribution (0.138), followed by vegetation protection loss (Vf) (0.133). Together, these two variables accounted for approximately 45.8% of the total WEPI, highlighting the dominant role of vegetation degradation and exposed soil surfaces in controlling wind erosion potential. Soil moisture dryness (SMf), land surface temperature (LSTf), precipitation dryness (Pdry), soil erodibility (SoilE), wind force (WF), land-cover exposure (LCF), and topographic susceptibility (TopoF) made smaller but still meaningful contributions to the index. Sensitivity analysis demonstrated that the spatial distribution of WEPI remained highly consistent across alternative weighting schemes, with correlation coefficients ranging from 0.933 to 0.986 relative to the primary extended balanced model. However, the estimated proportion of the study area classified as high or very high risk varied from 16.45% under the climate-driven weighting scheme to 27.78% under the surface-driven scheme. These results indicate that although the spatial pattern of wind erosion potential is robust, the estimated extent of high-risk areas is influenced by the relative weighting assigned to climatic and surface-related variables(Zhang et al., 2025).

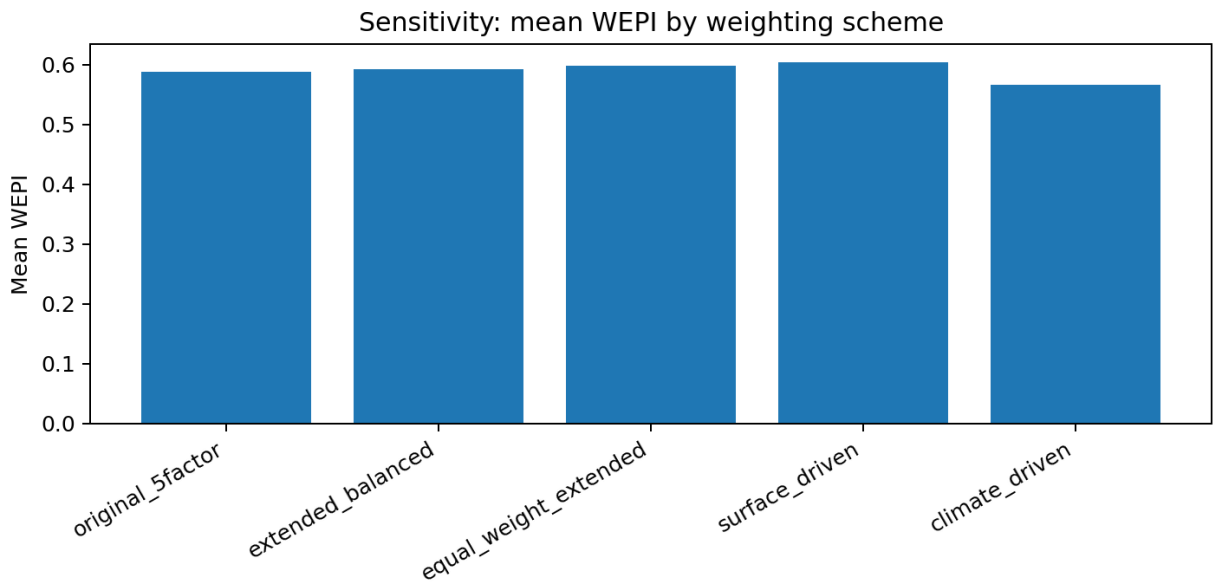


Figure 6. Component contributions to the Wind Erosion Potential Index (WEPI) and sensitivity of WEPI to alternative weighting schemes.

Table 6. Component contributions and sensitivity of WEPI to alternative weighting schemes.

Variable / scheme	**Key result**
BSI weighted contribution	0.138
Vf weighted contribution	0.133
SMf weighted contribution	0.070
LSTf weighted contribution	0.062
Pdry weighted contribution	0.049
SoilE weighted contribution	0.042
WF weighted contribution	0.041
LCF weighted contribution	0.029
TopoF weighted contribution	0.027
Original five-factor mean WEPI	0.588
Extended balanced mean WEPI	0.592

Variable / scheme	Key result
Equal-weight extended mean WEPI	0.598
Surface-driven mean WEPI	0.604
Climate-driven mean WEPI	0.566
Correlation range with primary model	0.933–0.986

3.5. Trend, endpoint change, hotspots, and priority zones

Pixel-wise trend analysis indicated a weak overall increase in wind erosion potential during 2016–2025. The mean Theil–Sen slope was 0.0016 WEPI yr^{-1}, while the median slope reached 0.0019 WEPI yr^{-1}. Nevertheless, statistically significant increasing trends were identified in only 125 pixels, representing 0.18% of all valid pixels. Figure 7 illustrates that most of the province exhibited no significant monotonic trend, whereas localized areas showed increasing wind erosion potential.

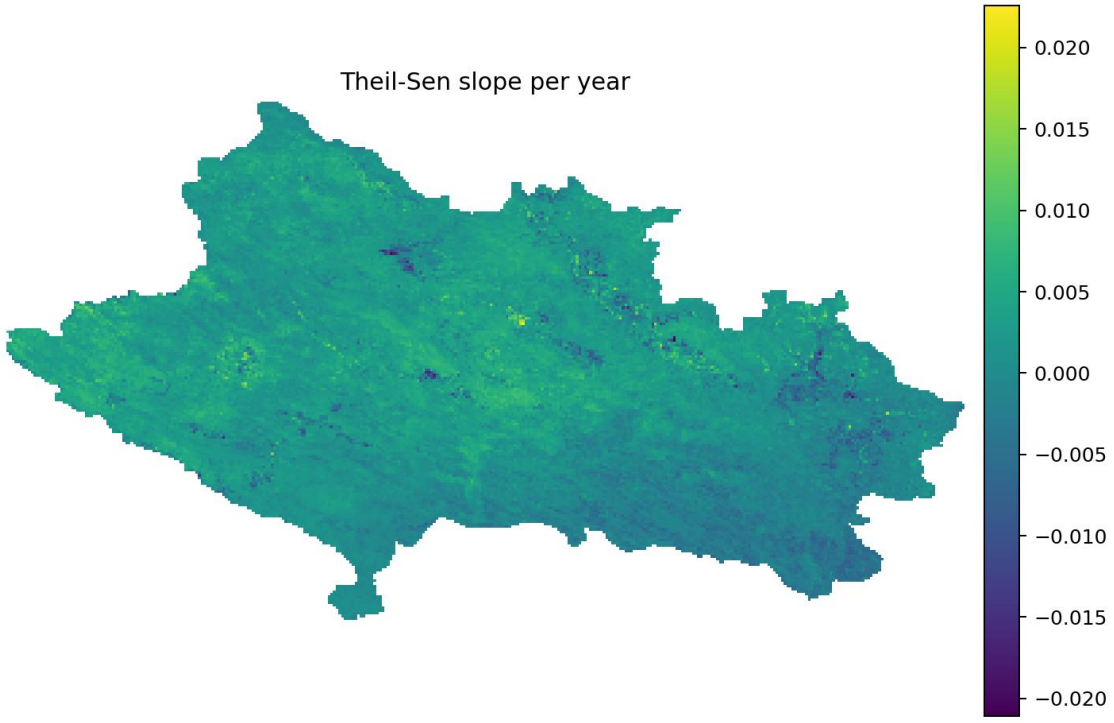


Figure 7. Pixel-wise WEPI trend analysis.

Endpoint analysis indicated a slight overall increase in WEPI between 2016 and 2025. The mean ΔWEPI_(2025–2016) was +0.0126, with values ranging from −0.2010 to +0.2274. Sensitivity analysis demonstrated that the mean endpoint change for 2016–2024 was substantially smaller (+0.0012), whereas the 2017–2025 interval produced a slightly larger value (+0.0152). These results suggest that endpoint differences are influenced by the selected time interval and therefore primarily reflect localized changes rather than a province-wide shift which can be seen in Figure 8.

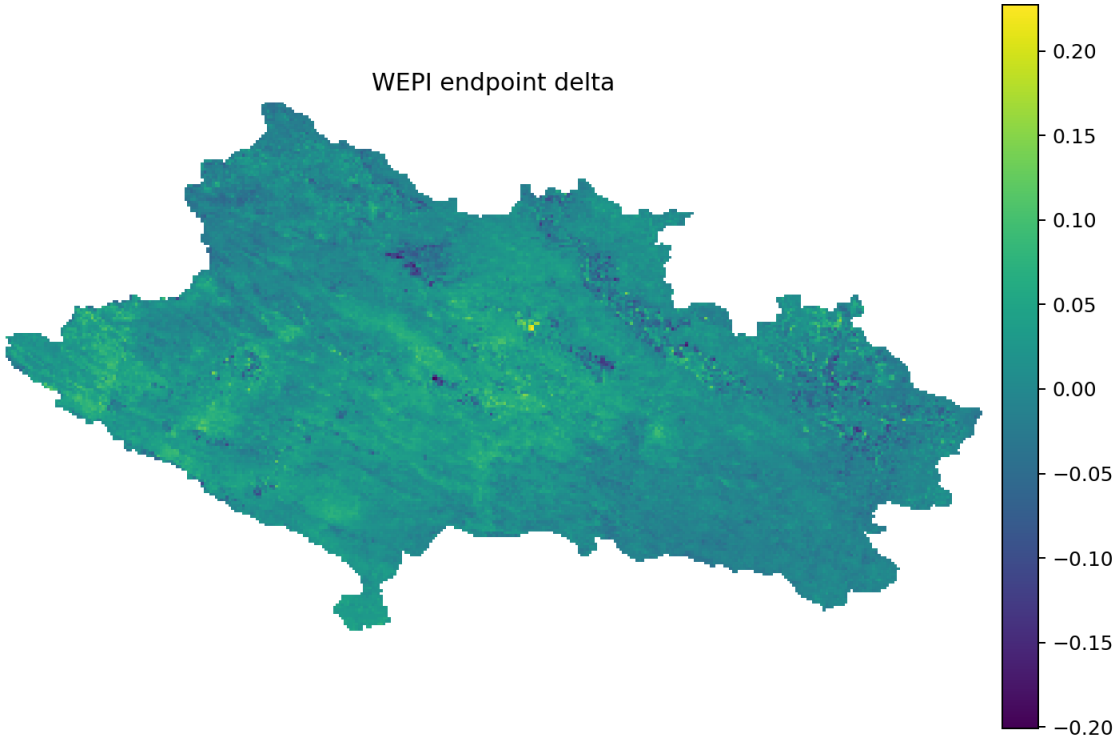


Figure 8. Endpoint change in WEPI.

Spatial clustering analysis using the Getis–Ord Gi* statistic identified 12,804 hotspot pixels and 14,006 coldspot pixels (Figure 9). High-risk persistence analysis further identified 17,366 pixels that repeatedly remained within the high or very high WEPI classes throughout the study period. These findings indicate that persistent erosion-prone areas were considerably more extensive than areas exhibiting statistically significant increasing trends.

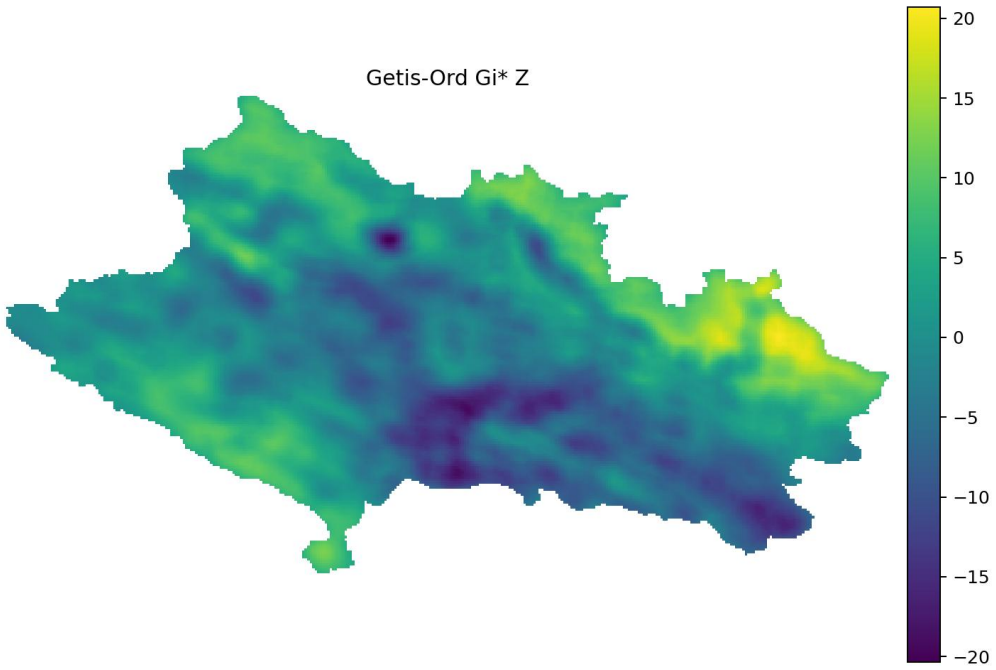


Figure 9. Spatial clustering and persistence of WEPI.

The management-priority map integrated long-term mean WEPI, hotspot occurrence, significant increasing trends, endpoint change, high-risk persistence, and data quality. Figure 10 shows that the highest-priority zones were characterized by high erosion potential, significant spatial clustering, persistent high-risk conditions, and localized increasing trends. These areas represent the highest priorities for wind erosion monitoring, rangeland management, vegetation restoration, and soil-surface stabilization (Lackóová & Tárníková, 2026).

The disparity between the limited extent of statistically significant increasing trends (0.18% of valid pixels) and the vast extent of persistent high-risk areas highlights a critical characteristic of wind erosion in Lorestan Province. The lack of widespread, monotonic increases in WEPI does not imply an improving landscape; rather, it indicates that erosion susceptibility has already reached a high and stable baseline across much of the province. The endpoint change analysis further supports this, demonstrating that while province-wide shifts are modest, localized areas are experiencing accelerated degradation depending on the observed time interval. Consequently, environmental monitoring must prioritize the management of these chronically exposed zones rather than solely searching for emerging areas of rapid deterioration.

Comparable multi-temporal analyses in semi-arid landscapes have shown that remotely sensed vegetation, soil, salinity, and temperature indicators can reveal persistent land-degradation and aeolian-erosion hotspots (Badapalli et al., 2026).

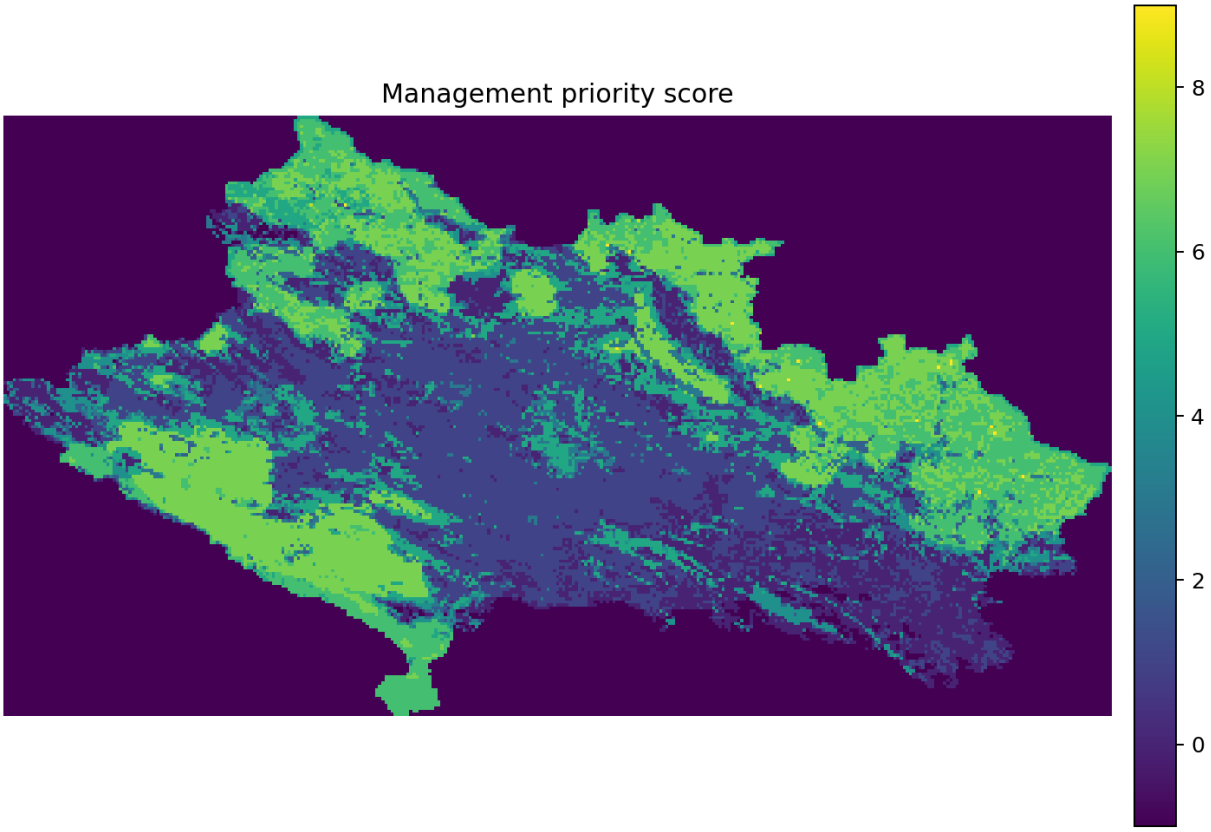


Figure 10. Management-priority zoning map for wind erosion mitigation in Lorestan Province.

The seasonal surge in wind erosion potential during the summer and early autumn (mean WEPI of 0.633 in JJA) reflects a critical convergence of climatic forcing and anthropogenic land use. During these warm, dry months, the natural senescence of vegetation and depletion of soil moisture are frequently compounded by post-harvest agricultural clearing and intensive rangeland grazing. Because Lorestan features diverse agricultural and rangeland systems interspersed within mountainous terrain, human-induced surface exposure effectively amplifies the region's inherent climatic vulnerabilities. The high component contributions of bare soil exposure and vegetation protection loss to the overall WEPI validate this dynamic, confirming that seasonal land-cover transitions are the primary catalysts for localized wind erosion events.

Overall, the results indicate that Lorestan Province experienced persistent moderate-to-high wind erosion potential throughout the 2016–2025 period. Bare soil exposure and vegetation protection loss emerged as the dominant controls of WEPI, while seasonal analysis indicated the highest erosion potential during summer and early autumn. Although statistically significant increasing trends were limited and spatially localized, hotspot and persistence analyses demonstrated that large portions of the province consistently remained vulnerable to wind erosion, highlighting priority areas for long-term monitoring and land degradation mitigation. The principal trend, endpoint-change, spatial-clustering, and persistence metrics are summarized in Table 7.

Table 7. Summary of temporal trends, endpoint change, spatial clustering, and high-risk persistence of WEPI.

Indicator	**Result**
Mean Theil-Sen slope	0.0016 WEPI yr^{-1}
Median Theil-Sen slope	0.0019 WEPI yr^{-1}
Significant increasing pixels	125
Significant increasing pixels, full grid	0.18%
Mean $\Delta WEPI_{2025-2016}$	+0.0126
Median $\Delta WEPI_{2025-2016}$	+0.0118
Min $\Delta WEPI_{2025-2016}$	−0.2010
Max $\Delta WEPI_{2025-2016}$	+0.2274
Mean $\Delta WEPI_{2016-2024}$	+0.0012
Mean $\Delta WEPI_{2017-2025}$	+0.0152
Hotspot pixels	12,804
Coldspot pixels	14,006
High-risk persistence pixels	17,366

4. Conclusion

This study developed and applied an extended multi-source Wind Erosion Potential Index (WEPI) framework to evaluate the spatial and temporal dynamics of wind erosion potential in Lorestan Province, western Iran, during 2016–2025. By integrating satellite observations, climate reanalysis, soil properties, topographic characteristics, and land-cover information within the Google Earth Engine and Python environments, the proposed framework provided a comprehensive and spatially explicit assessment of wind erosion susceptibility. The combination of multi-source environmental datasets with statistical trend analysis, hotspot detection, persistence mapping, and sensitivity analysis offers a reproducible approach for regional-scale wind erosion assessment.

The results demonstrated that wind erosion potential was persistent and spatially widespread throughout the study period. The long-term mean WEPI was approximately 0.592, indicating that much of the province experienced moderate-to-high erosion potential. Risk classification further confirmed this pattern, with more than 95% of the valid study area repeatedly classified as moderate, high, or very high risk. These findings suggest that wind erosion in Lorestan is not restricted to isolated locations but represents a widespread land-degradation concern affecting large portions of the province.

Seasonal analysis revealed a clear temporal pattern in erosion susceptibility. Wind erosion potential was lowest during winter and spring and increased markedly during summer and early autumn, when vegetation cover declined, soil moisture decreased, and bare soil exposure became more extensive. The highest WEPI values occurred during the summer months, highlighting this period as the most critical season for wind erosion monitoring and mitigation. These seasonal dynamics emphasize the importance of considering temporal variability when designing land management and conservation strategies.

Component contribution analysis showed that bare soil exposure and vegetation protection loss were the dominant controls of the WEPI, together accounting for nearly 46% of the total index. This finding underscores the fundamental role of land-surface conditions in controlling wind erosion susceptibility. Although climatic variables, soil erodibility, land-cover characteristics, and

topographic conditions also contributed to the index, their individual influence was comparatively smaller. Consequently, management strategies that reduce bare soil exposure and improve vegetation cover are likely to provide the greatest benefits for mitigating wind erosion risk in the region.

Sensitivity analysis demonstrated that the proposed WEPI framework is robust with respect to alternative weighting schemes. Spatial correlations between the primary model and alternative weighting scenarios remained consistently high, indicating that the overall spatial distribution of wind erosion potential was stable. Although the estimated extent of high-risk areas varied depending on the weighting strategy, the principal erosion-prone zones remained largely unchanged. This robustness increases confidence in the applicability of the proposed framework for regional assessment and environmental decision-making.

Trend analysis indicated only a weak overall increase in wind erosion potential during the study period. Statistically significant increasing trends were confined to a relatively small proportion of the study area, suggesting that widespread monotonic degradation has not yet occurred. Likewise, endpoint change analysis indicated only a modest overall increase, with localized areas exhibiting stronger positive changes. In contrast, hotspot and persistence analyses revealed that large areas consistently remained within high-risk categories throughout the study period. These findings indicate that persistent erosion susceptibility represents a more important management concern than widespread temporal intensification.

The integration of hotspot analysis, persistence mapping, and management-priority assessment provides valuable information for land degradation management. Areas characterized by high mean WEPI, persistent high-risk conditions, statistically significant spatial clustering, and localized increasing trends should be considered priority zones for monitoring and mitigation. In Lorestan Province, practical management measures should focus on vegetation restoration, rangeland conservation, reducing bare soil exposure, stabilizing vulnerable soil surfaces, and strengthening erosion-control practices during the summer and early autumn when erosion potential reaches its maximum.

The proposed WEPI framework represents an advance over conventional wind erosion assessments by integrating multiple environmental controls within a unified spatiotemporal modeling framework. Because the methodology relies primarily on globally available satellite,

climate, soil, terrain, and land-cover datasets, it can be readily transferred to other semi-arid and mountainous regions facing similar land degradation challenges. This transferability makes the framework suitable for supporting regional environmental monitoring and sustainable land management beyond the study area.

Moving beyond broad regional assessments, the management-priority zoning map provides an actionable, spatially explicit blueprint for resource allocation. By synthesizing long-term WEPI means, hotspot clustering, and high-risk persistence, the resulting priority score effectively isolates the landscapes requiring immediate intervention. For regional planners in Lorestan Province, these highest-priority zones represent optimal locations for targeted investments in sustainable land management (SLM) practices. Interventions in these specifically delineated areas—such as regulating seasonal grazing intensities, implementing post-harvest stubble retention, and restoring degraded rangeland vegetation—will yield the highest return on investment for mitigating wind erosion and combating localized desertification.

Despite these strengths, the present study estimates wind erosion potential rather than directly measuring soil loss or sediment transport. Therefore, future research should validate WEPI using field observations, dust-event inventories, erosion measurements, and local meteorological records. Additional improvements may include incorporating higher-resolution wind datasets, dynamic soil crust information, and machine learning approaches for optimizing variable weighting. Such developments would further strengthen the predictive capability of the framework and enhance its usefulness for operational wind erosion monitoring under changing climatic and land-use conditions.

Author contribution
Mostafa Ghasemzadeh: data acquisition and preparation, methodology implementation, modeling setup, software application, formal analysis, visualization, and result presentation.
Meysam Bali: conceptualization, development of the original idea and study scope, methodology validation, manuscript preparation, review, and editing.

Data availability:Processed data and model outputs are available from the corresponding author upon reasonable request.

Declarations
Ethical approval: The authors have observed all ethical responsibilities.

Consent to publish: Not applicable.
Competing interests: The authors declare no competing interests.
Funding: This research received no external funding

References

Badapalli, P. K., Nakkala, A. B., Kottala, R. B., Pujari, P. S., & Gugulothu, S. (2026). Aeolian sand migration induced land degradation and desertification hotspots identification in the semi-arid rain shadow regions of Anantapur, India. *Scientific Reports, 16*, 1875. https://doi.org/10.1038/s41598-025-31610-0

Benjamini, Y., & Hochberg, Y. (1995). Controlling the false discovery rate: A practical and powerful approach to multiple testing. Journal of the Royal Statistical Society: Series B (Methodological), 57(1), 289–300. https://doi.org/10.1111/j.2517-6161.1995.tb02031.x

Chao, Y., Zhu, Y., Wang, X., Li, J., & Liang, L. (2025). Dynamic evolution of the NDVI and driving factors in the Mu Us Sandy Land of China from 2002 to 2021. *Journal of Arid Land, 17*, 605–623. https://doi.org/10.1007/s40333-025-0052-4

Drusch, M., Del Bello, U., Carlier, S., Colin, O., Fernandez, V., Gascon, F., Hoersch, B., Isola, C., Laberinti, P., Martimort, P., Meygret, A., Spoto, F., Sy, O., Marchese, F., & Bargellini, P. (2012). Sentinel-2: ESA's optical high-resolution mission for GMES operational services. Remote Sensing of Environment, 120, 25–36. https://doi.org/10.1016/j.rse.2011.11.026

Entekhabi, D., Njoku, E. G., O'Neill, P. E., Kellogg, K. H., Crow, W. T., Edelstein, W. N., Entin, J. K., Goodman, S. D., Jackson, T. J., Johnson, J., Kimball, J., Piepmeier, J. R., Koster, R. D., Martin, N., McDonald, K. C., Moghaddam, M., Moran, S., Reichle, R. D., Shi, J. C., Spencer, M. W., Thurman, S. W., Tsang, L., & Van Zyl, J. (2010). The Soil Moisture Active Passive mission. Proceedings of the IEEE, 98(5), 704–716. https://doi.org/10.1109/JPROC.2010.2043918

Farr, T. G., Rosen, P. A., Caro, E., Crippen, R., Duren, D., Hensley, S., Kobrick, M., Paller, M., Rodriguez, E., Roth, L., Seal, D., Shaffer, S., Shimada, J., Umland, J., Werner, M., Oskin, M., Burbank, D., & Alsdorf, D. (2007). The Shuttle Radar Topography Mission. Reviews of Geophysics, 45(2), RG2004. https://doi.org/10.1029/2005RG000183

Feizizadeh, B., Yariyan, P., Yakar, M., Blaschke, T., & Saif Almuraqab, N. A. (2025). An integrated hybrid deep learning data driven approaches for spatiotemporal mapping of land susceptibility to salt/dust emissions. *Advances in Space Research, 75*(10), 7112–7134. https://doi.org/10.1016/j.asr.2025.02.047

Feng, Y., Ding, J., Bao, A., & Li, J. (2025). Attribution and risk assessment of wind erosion in the Aral Sea regions using multi-source remote sensing and RWEQ on GEE. *Remote Sensing, 17*(16), 2788. https://doi.org/10.3390/rs17162788

Funk, C., Peterson, P., Landsfeld, M., Pedreros, D., Verdin, J., Shukla, S., Husak, G., Rowland, J., Harrison, L., Hoell, A., & Michaelsen, J. (2015). The climate hazards infrared precipitation with stations—A new environmental record for monitoring extremes. Scientific Data, 2, 150066. https://doi.org/10.1038/sdata.2015.66

Getis, A., & Ord, J. K. (1992). The analysis of spatial association by use of distance statistics. Geographical Analysis, 24(3), 189–206. https://doi.org/10.1111/j.1538-4632.1992.tb00261.x

Gholami, H., Mohammadifar, A., Song, Y., Li, Y., Rahmani, P., Kaskaoutis, D. G., Panagos, P., & Borrelli, P. (2024). An assessment of global land susceptibility to wind erosion based on deep-active learning modelling and interpretation techniques. *Scientific Reports, 14*, 18951. https://doi.org/10.1038/s41598-024-70125-y

Gorelick, N., Hancher, M., Dixon, M., Ilyushchenko, S., Thau, D., & Moore, R. (2017). Google Earth Engine: Planetary-scale geospatial analysis for everyone. Remote Sensing of Environment, 202, 18–27. https://doi.org/10.1016/j.rse.2017.06.031

Hengl, T., Mendes de Jesus, J., Heuvelink, G. B. M., Ruiperez Gonzalez, M., Kilibarda, M., Blagotić, A., Shangguan, W., Wright, M. N., Geng, X., Bauer-Marschallinger, B., Guevara, M. A., Vargas, R., MacMillan, R. A., Batjes, N. H., Leenaars, J. G. B., Ribeiro, E., Wheeler, I., Mantel, S., & Kempen, B. (2017). SoilGrids250m: Global gridded soil information based on machine learning. PLOS ONE, 12(2), e0169748. https://doi.org/10.1371/journal.pone.0169748

Kendall, M. G. (1975). Rank correlation methods (4th ed.). Charles Griffin.

Khoshnoud, S., Mirmazloumi, S. M., Ghorbanian, A., Asgari, H. M., & Amani, M. (2026). Mapping wind erosion potential using remote sensing and artificial neural networks: Insights for

soil conservation in arid regions. *Remote Sensing Applications: Society and Environment, 41*, 101804. https://doi.org/10.1016/j.rsase.2025.101804

Lackóová, L., & Tárníková, M. (2026). Identifying priority areas for wind erosion prevention through GIS-based suitability analysis. *Frontiers in Agronomy, 8*, 1822170. https://doi.org/10.3389/fagro.2026.1822170

Li, R., Pei, H., Zhang, S., Li, F., Lin, X., Wang, S., & Yang, L. (2023). Dividing the transit wind speeds into intervals as a favorable methodology for analyzing the relationship between wind speed and the aerodynamic impedance of vegetation in semiarid grasslands. *Journal of Arid Land, 15*, 887–900. https://doi.org/10.1007/s40333-023-0102-8

Mann, H. B. (1945). Nonparametric tests against trend. Econometrica, 13(3), 245–259. https://doi.org/10.2307/1907187

Mohammadi, M., Gholami, H., Mohamadifar, A., Song, Y., & Kaskaoutis, D. (2025). Enhancing wind erosion hazard assessment: A novel framework combining integrated land susceptibility to wind erosion index and machine learning algorithms—Case study of the Saravan area, Southeast Iran. *Aeolian Research, 74*, 100995. https://doi.org/10.1016/j.aeolia.2025.100995

Muñoz-Sabater, J., Dutra, E., Agustí-Panareda, A., Albergel, C., Arduini, G., Balsamo, G., Boussetta, S., Choulga, M., Harrigan, S., Hersbach, H., Martens, B., Miralles, D. G., Piles, M., Rodríguez-Fernández, N. J., Zsoter, E., Buontempo, C., & Thépaut, J.-N. (2021). ERA5-Land: A state-of-the-art global reanalysis dataset for land applications. Earth System Science Data, 13, 4349–4383. https://doi.org/10.5194/essd-13-4349-2021

Okin, G. S. (2008). A new model of wind erosion in the presence of vegetation. Journal of Geophysical Research: Earth Surface, 113, F02S10. https://doi.org/10.1029/2007JF000758

Ravi, S., D'Odorico, P., Breshears, D. D., Field, J. P., Goudie, A. S., Huxman, T. E., Li, J., Okin, G. S., Swap, R. J., Thomas, A. D., Van Pelt, S., Whicker, J. J., & Zobeck, T. M. (2011). Aeolian processes and the biosphere. Reviews of Geophysics, 49(3), RG3001. https://doi.org/10.1029/2010RG000328

Saeedi Nazarlu, F., Khavarian Nehzak, H., Mostafazadeh, R., & Alaei, N. (2026). Spatial hotspot analysis of soil erosion rate and classification of homogeneous zones using GIS in a mountainous

contrasting land-use watershed. *Scientific Reports, 16*, 10456. https://doi.org/10.1038/s41598-026-41668-z

Sen, P. K. (1968). Estimates of the regression coefficient based on Kendall's tau. Journal of the American Statistical Association, 63(324), 1379–1389. https://doi.org/10.1080/01621459.1968.10480934

Shao, Y., Wyrwoll, K. H., Chappell, A., Huang, J., Lin, Z., McTainsh, G. H., Mikami, M., Tanaka, T. Y., Wang, X., & Yoon, S. (2011). Dust cycle: An emerging core theme in Earth system science. Aeolian Research, 2(4), 181–204. https://doi.org/10.1016/j.aeolia.2011.02.001

Wan, Z. (2006). MODIS land surface temperature products users' guide. Institute for Computational Earth System Science, University of California, Santa Barbara.

Yang, W., Zhang, G., Yang, H., Lin, D., & Shi, P. (2023). Review and prospect of soil compound erosion. *Journal of Arid Land, 15*, 1007–1022. https://doi.org/10.1007/s40333-023-0107-3

Zanaga, D., Van De Kerchove, R., Daems, D., De Keersmaecker, W., Brockmann, C., Kirches, G., Wevers, J., Cartus, O., Santoro, M., Fritz, S., Lesiv, M., Herold, M., Tsendbazar, N.-E., Xu, P., & Ramoino, F. (2022). *ESA* WorldCover *10 m 2021 v200*. Zenodo. https://doi.org/10.5281/zenodo.7254221

Zhang, G., Ma, Y., Azorin-Molina, C., Minola, L., Wang, Y., Lin, Z., Ma, H., & Shi, P. (2025). An increase in wind erosion dominated by wind speed changes over the Tibetan Plateau from 1982 to 2020. *Science of the Total Environment, 998*, 180278. https://doi.org/10.1016/j.scitotenv.2025.180278